Effect of Photocatalytic Pretreatment on the Membrane Performance in Nanofiltration of Textile Wastewater

Sevde Korkut · Türkan Ormanci-Acar · Basak Keskin · Meltem Ağtaş ·
Özlem Karahan · Tuğba U. Demir · Serkan Unal · Yusuf Z. Menceloglu ·
Ismail Koyuncu

Abstract Traditional methods like biological treatment, flocculation-coagulation, adsorption, and advanced oxidation are commonly employed for textile wastewater treatment, but their sustainability is hindered by issues such as the adverse impact of textile wastewater on microorganisms and the requirement for substantial chemical usage. In response to increasingly stringent legal discharge standards, membrane technologies are emerging as prominent alternatives for effective textile wastewater treatment. The application of photocatalysis as a pretreatment to improve effluent quality and treatment performance has shown effective results in the treatment of textile wastewater by nanofiltration (NF). However, innovative solutions are needed to improve the efficiency of UV photocatalytic reactors. Here, the TiO_2/halloysite nanotube (HNT) photocatalyst was shown to completely remove dyes under UV illumination. Two wastewater samples from photocatalytic (PC) pretreatment were treated using innovative NF membranes with different contents. The study examined the impact of PC pretreatment on the flux of wastewater from a textile factory heat recovery tank, which increased from 18.32 to 27.63 $L/m^2.h$. The membranes achieved > 98% removal in COD, while bare membrane achieved 95% removal in conductivity. The addition of s-DADPS as monomer and HNT as nanoparticles to the membranes with different compositions affected the cross-linking in the TFC layer. During the tests conducted on the water extracted from the dyeing tank, the color was completely eliminated without any loss of flux. Additionally, improvements in COD removal were observed.

S. Korkut · T. Ormanci-Acar · B. Keskin · M. Ağtaş ·
I. Koyuncu (✉)
National Research Center On Membrane Technologies,
Istanbul Technical University, Istanbul, Turkey
e-mail: koyuncu@itu.edu.tr

S. Korkut · B. Keskin · I. Koyuncu
Faculty of Civil Engineering, Department
of Environmental Engineering, Istanbul Technical
University, Istanbul, Turkey

T. Ormanci-Acar
Faculty of Engineering, Department of Environmental
Engineering, Istanbul University-Cerrahpasa, Istanbul,
Turkey

Ö. Karahan
The Scientific and Technological Research Council
of Turkey (TUBITAK), Marmara Research Center,
Gebze, Kocaeli, Turkey

T. U. Demir
ESAN Eczacibasi, Istanbul, Turkey

S. Unal · Y. Z. Menceloglu
Faculty of Engineering and Natural Sciences, Material
Science and Nanoengineering, Sabanci University,
Istanbul, Turkey

S. Unal · Y. Z. Menceloglu
Integrated Manufacturing Technologies Research
and Application Center, Composite Technologies Center
of Excellence, Sabanci University, Istanbul, Turkey

1 Introduction

One of the biggest challenges of the twenty-first century is the supply of adequate clean water for drinking water, industrial use, and sanitation. In addition to the fact that clean water is indispensable for vital activities, the rapid increase in the world population and industrialization also force natural resources. A wide variety of industries such as cosmetics, pulp and paper, and textiles, in addition to high water consumption for their processes, also cause the production of highly polluted wastewater (Ağtaş et al., 2020).

When various industries are compared, the textile industry stands out as one of the industries that produce the highest amount of wastewater. It has been reported that more than half (54%) of dye waste discharged into the environment worldwide originates from the textile industries. In addition, it is known that the dyes used in the textile industry are quite harmful to aquatic life and the environment. In this context, owing to the efficient treatment and reuse of textile wastewater, it is possible to reduce both the pollution load given to the environment and the clean water used by the textile industry (Agtaş et al., 2021).

Many traditional wastewater treatment methods such as biological treatment, flocculation-coagulation, adsorption, and advanced oxidation are widely used in the treatment of textile wastewater. However, traditional treatment methods cannot be sustainable in textile wastewater treatment due to reasons such as the content of textile wastewater affecting microorganisms or the need for high amounts of chemicals for effective treatment (Li et al., 2019). Considering the tightening of legal discharge standards day by day, membrane technologies come to the fore for textile wastewater treatment. In addition, membranes have high efficiency in treatment, need low space, and are highly effective in chemical and water recovery, making membranes an important option for textile wastewater treatment (Keskin et al., 2021a).

Photocatalysis, one of the advanced oxidation techniques, is used to decompose dye compounds using hydroxyl radicals and convert them into components such as mineral acids, water, and carbon dioxide.

Various semiconductor materials such as ZnO (Aftab et al., 2022; Qi et al., 2017), CeO_2 (Iqbal et al., 2022), ZnS (Hu et al., 2005), quantum dots (Korkut et al., 2023), metallic doped TiO_2 (Ahmadpour et al., 2024), g-C3N4 (Qamar et al., 2023), vanadium oxide (V_2O_5) (Naseem & Durrani, 2021), and tin oxide (SnO_2) (Ahmad et al., 2023) have been employed for the photocatalytic oxidation of organic substance. Among these materials, titania (TiO_2) stands out with its low cost, high photocatalytic activity, and inert and chemical stability (Das & Basu, 2015). Titania particles must be removed from the effluent after the process has been carried out. However, since the particles are quite small in size, they are difficult to recover. Therefore, titania can be immobilized on various support materials such as cellulose fibers, various adsorbents, glass, and carbon (Alinsafi et al., 2007). In a study carried out to degrade textile dyes by photocatalytic method and to reduce their toxicity, immobilized titania was used. In this pilot-scale study, Acid Blue 25 dye was chosen as the main pollutant. In light of the data obtained, it has been reported that the target dye can compose and its toxicity can be reduced (Mahmoodi & Arami, 2009). In another study in which iron-doped titania was positioned on graphene oxide, the photocatalytic performance was investigated using Rhodamine B. As a result of the experiments, it was stated that the best Rhodamine B removal was found to be 91% after 120 min. It was underlined that a significant total organic carbon (TOC) and chemical oxygen demand (COD) removal was achieved in studies with real textile wastewater (Isari et al., 2018). Because of their porous surface, low cost, mechanical and chemical resistance, and tubular construction, TiO_2/HNT nanocomposites (Fig. 1) have a lot of potential for eliminating water pollutants (Du & Zheng, 2014; Jiang et al., 2015; Mishra & Mukhopadhyay, 2019; Wang et al., 2011; Zheng et al., 2015). Dyes used in photocatalytic tests are mostly used in the textile and dye industry and are removed by adsorption and/or degradation (Abid et al., 2023).

Fluidized bed application is an application that has attracted attention in recent years in studies related to the coating of TiO_2 on support materials. In this application, the balls of support material coated with TiO_2 are usually "vented" in the reactor with the flow of water or gas supplied from the side or bottom of the reactor, allowing the bed to flow in the reactor. Thus, the system in which TiO_2 is

applied in suspension is imitated and the advantages of using TiO_2 in a supported manner are utilized. In the studies on the applications of TiO_2 in the fluidized bed reactor, such as quartz sand, sintered glass, which are less adsorptive, or different types of activated carbon which are high-capacity adsorptive materials have been used (Baek et al., 2013; Haarstrick et al., 1996; Kanki et al., 2005; Pozzo et al., 2011).

To the best of our knowledge, there is no study in the literature using TiO_2/HNT nanoparticles in UV-C photocatalytic reaction and directly with real textile wastewater. In the scope of this study, photocatalytic treatment and nanofiltration membranes and configurations have been tested for the treatment of cotton textile industry wastewaters which have been dyed at high temperature and alkaline conditions. In these experiments, real textile wastewater and photocatalytic reactor effluent were used. Then, NF membranes were tested to provide high flux, high dye, and divalent salt removal in real wastewater.

2 Material and Methods

This study consists of three main parts. These are UV photocatalytic pretreatment, NF membrane production, and NF application with real textile wastewater. In order to reveal the difference in pretreatment, a NF experiment set was conducted without pretreatment. The details of the methods used are explained in this section.

2.1 Wastewater Characteristics

Two samples of textile wastewater (WW) were used in this research. Heat recovery tank WW and printing WW obtained from a cotton textile factory in Turkey. The characteristics of wastewater is given in Table 1. Filtration tests were performed under 9 bar for 1 h constantly.

2.2 Reagents and Chemicals

HNT (halloysite nanotube) was supplied from Esan-NANO Group (Turkey) as 5 μm average in size. Detailed information about HNTs was given in our previous study (Keskin et al., 2021b). HNT was used in both fluidized bed photoreactor and membrane production. Hydrochloric acid (HCl, 36.5–38%) was purchased from Sigma-Aldrich, Ltd. Titanium (IV)

Table 1 Characterization of real textile wastewaters

Parameter	Unit	Heat recovery WW	Printing WW
		Value	Value
pH	-	11.5	11.7
COD	mg/L	3486	996
Conductivity	μs/cm	3400	8869
Color			
Pt–Co		127	239
436 nm	abs	0.344	0.575
525 nm		0.279	0.470
620 nm		0.338	0.501
CN		0.323	0.519

Fig. 1 Schematic structure of TiO_2/HNT
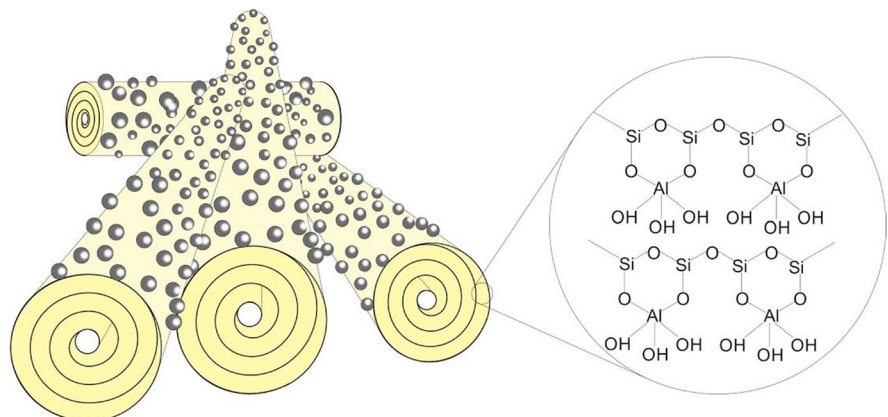
isopropoxide (TTIP, Ti[OCH(CH$_3$)$_2$]$_4$) was purchased from Alfa Aesar.

For the production of ultrafiltration membrane, polysulfone (PSf, Udel® P-3500) was purchased from Solvay Specialty Polymers, USA. N-Methyl 2-pyrrolidinone (NMP) which was a solvent was bought from Ashland (USA).

To fabricate thin films, disodium-3–3′-disulfonate-4–4′-dichloro-diphenyl sulfone (s-DCDPS) was provided from Akron Polymer Systems, USA. N, N-dimethylacetamide (DMAc) and toluene were obtained from Sigma-Aldrich. 3-aminophenol (m-AP) was bought from Sigma-Aldrich and dried before use. Potassium carbonate and isopropyl alcohol were purchased from Sigma-Aldrich, Ltd. Also disodium 3–3′-disulfonate-bis[4-(3-aminophenoxy) phenyl] sulfone (s-DADPS) was synthesized by using these chemicals. Trimesoyl chloride (or 1,3,5-benzenetricarbonyl trichloride, TMC, 98%), anhydrous piperazine (PIP, ≥ 99.0%), and anhydrous cyclohexane (≥ 99.0%) were purchased from Sigma-Aldrich, Ltd. Reactive Orange (Mw: 617.54 g/mol) was purchased from Sigma-Aldrich, Ltd. Setazol Red reactive dye (Mw: 1469.98 g/mol) was kindly donated by Setas Chemicals, Tekirdag, Turkey. All experiments were conducted with ultrapure water.

2.3 Fluidized Bed Photoreactor and NF Hybrid System

2.3.1 Preparation and Characterization of TiO$_2$/HNT Photocatalyst by Hydrothermal Method

The HNT nanotubes were dried at 110 °C for about 12 h. In this way, the water molecules between the layers are irreversibly removed. A one-step hydrothermal method was used to coat the HNT with TiO$_2$ nanoparticles (Wang et al., 2011). Using titanium (IV) isopropoxide (1.73 mL) (TTIP, Ti[OCH(CH$_3$)$_2$]$_4$, Alpha Aesar) as the initiator alkoxide, it was dissolved in 20 mL isopropanol (IPA, C$_3$H$_8$O, Aldrich) and stirred at room temperature for 2 h. On the other hand, HNT (1 gr) was added to 20 mL isopropanol, and the particles were dispersed in the solvent for 30 min by applying 40% power with the help of probe sonication (Qsonica Ultrasonic Processor—maximum power 700 W). Both mixtures were brought together in a Teflon container and adjusted to pH 4 with the aid of 6 M hydrochloric acid. As it is known, when

the surface of the TiO$_2$ catalyst is less than 6.3, the surface is positively charged (Evgenidou et al., 2005). However, the surface of HNT is negatively charged when pH < 2.4. Thus, positively charged particles can be easily absorbed onto HNT and decomposed effectively (Abdullayev et al., 2009). In this study, it is aimed to work at pH 4 as suggested in the literature (Wang et al., 2011). Then, the lid of the Teflon container was tightly closed, placed in a stainless steel autoclave, and kept in the oven set at 150 °C for 24 h. Afterwards, it was cooled to room temperature, removed from the steel autoclave, and washed 3 times with 5 mL of water (first by vortexing and then centrifuging at 4200 rpm for 5 min). TiO$_2$/HNT composites in the form of white solid obtained were dried in an oven set at 110 °C for 12 s after grinding in agate mortar until they became fine powder.

The structure and morphology of raw HNTs and HNTs coated with TiO$_2$ (TiO$_2$/HNTs) photocatalysts were characterized by field-emission scanning electron microscopy (FE-SEM)(FEG-SEM Zeiss Leo Supra 35VP) and high-resolution transmission electron microscopy (HRTEM) (JEOL ARM 200 CF microscope with aberration-corrected probe and accelerating voltage of 200 kV).

2.3.2 Photocatalytic Degradation Experiments

The UV reactor assembly for the fluidized bed photoreactor system was built in Turkey by a company experienced in reactor preparation. In order to ensure maximum efficiency in the reactor, an internally illuminated model was prepared, which is more suitable for the fluidized bed system (Braham & Harris, 2009). The schematic of the designed reactor can be seen in Fig. 2c. The ready state of the reactor is also given in Fig. 2a, b. In the interior of the reactor, there is a quartz sheet in which the lamp to be used to activate the photocatalyst and to provide illumination from the inside is placed. The lamp used in the reactor is a UV-C lamp with a power of 42 W and a luminous intensity of 110 μW/cm^2 at 1 m (LightTech, Austria). According to the data provided by the manufacturer, the lamp emits peak UV radiation at 253.7 nm. By giving dry air to the system, both the TiO$_2$/HNT photocatalysts were aerated and the solution was mixed, and the oxygen needed in the photocatalytic reaction was provided to the reactor.

Fig. 2 Images of the fluidized bed photoreactor (**a**, **b**), detailed schematic figure of reactor (**c**)
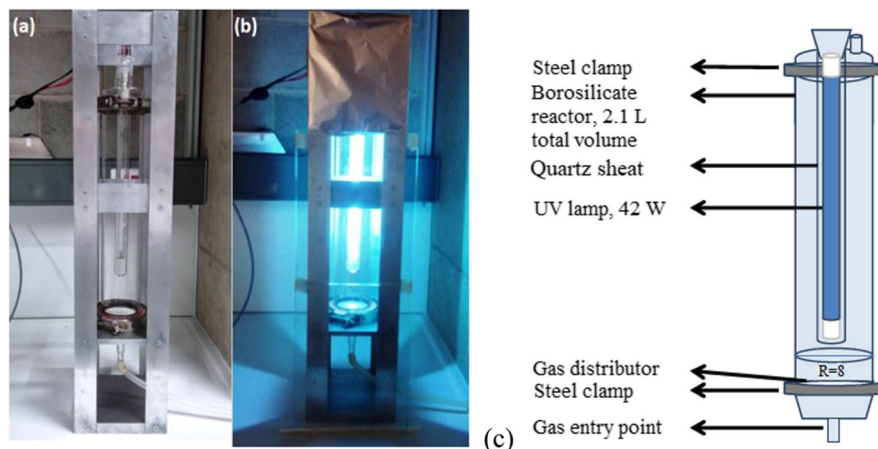
Reactive orange (RO16, Mw: 617.54 g/mol) and setazol red (SR120, Mw: 1469.98 g/mol) chemical dyes were used as model reactive dyes for raw HNT and TiO_2/HNT (2 g/L) adsorption and photocatalytic activity tests. Their chemical structures are given in Fig. 3. The initial concentrations of RO16 and SR120 were 100 mg/L and 200 mg/L. The solutions of dyes were prepared using ultrapure water. Prior to the photocatalytic activity test, the sample was stirred in the dark for 24 h to reach an adsorption–desorption equilibrium. An adsorbent-free experimental set was utilized for the direct UV light activity test. After stirring for 24 h, the UV light was turned on in the adsorbent-containing experimental sets. At some time intervals (about 1 h), dye concentrations were evaluated using a UV–vis spectrophotometer.

2.4 Fabrication of NF Membranes

As the support layer, a polysulfone (PSf)-based porous membrane was used for the interfacial

polymerization (IP) and fabricated as indicated in our previous study (Ormanci-Acar et al., 2020).

2.4.1 Fabrication of NF Membrane Containing HNT

First of all, for preparing an aqueous solution, 2% w/v PIP was added and dissolved in distilled water and 0.2% w/v TMC was dissolved in anhydrous hexane to get an organic phase solution at ambient temperature. HNTs were added into the aqueous phase and dispersed by probe sonication for 0.02% HNT TFN membranes. In the fabrication of 0.04% cycloHNT TFN membrane, HNT was added into TMC containing cyclohexane phase that has a higher polarity than hexane, a typical solvent used in TFC fabrication by interfacial polymerization, and thus provided a better dispersion before adding TMC. This process was carried out for 2 h at 90 watts before adding PIP. For 2 min, a side of the PSf support membrane was soaked in the aqueous phase solution by using a Plexiglas frame. The excess aqueous solution was decanted. Then, the same side of the support layer
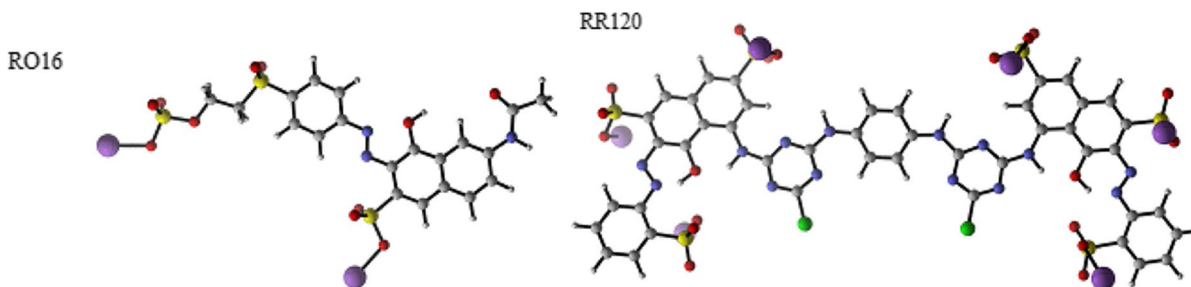
Fig. 3 Chemical structure of RO16 and SR120

saturated with the aqueous-phase solution was soaked with the organic-phase solution for 60 s. The membrane was kept in an oven at 70 °C for 5 min to make the membrane surface more stable, after removing the excess organic solution by decanting. As a final step, membranes were rinsed with distilled water and stored in distilled water at 4 °C before characterization tests.

2.4.2 Fabrication of NF Membrane with Containing s-DADPS

For fabricating 80% s-DADPS TFC NF membrane, 0.4% w/v PIP and 1.6% w/v s-DADPS were mixed and dissolved in distilled water. To prepare the organic phase solution, 0.2% w/v TMC was dissolved in anhydrous hexane at ambient temperature. A side of the PSf support was put in the aqueous phase solution for 2 min. The excess aqueous solution was decanted. Then, the same side of the support layer saturated with the aqueous-phase solution was put in the organic-phase solution for 60 s. The membrane was kept in an oven at 70 °C for 5 min to make the membrane surface more stable after removing the excess organic solution. As a final step, membranes were thoroughly rinsed with distilled water and stored in distilled water at 4 °C before characterization tests.

2.4.3 Fabrication of NF Membrane with Containing s-DADPS and HNT

To fabricate 80% s-DADPS 0.01% HNT TFN NF membrane, 0.4% w/v PIP and 1.6% w/v s-DADPS were put and dissolved in distilled water. For preparing the organic phase solution at room temperature, 0.2% w/v TMC was dissolved in anhydrous hexane. HNTs were added into the aqueous phase and dispersed by probe sonication for 2 h at 90 watts before adding PIP. One side of the PSf support membrane was soaked in the aqueous phase solution for 2 min. The excess aqueous solution was decanted. Then, the same side of the support layer saturated with the aqueous-phase solution was soaked with the organic-phase solution for 60 s. After removing the excess organic solution by decanting, the membrane was kept in an oven at 70 °C for 5 min to make the membrane surface more stable. As a final step, membranes were thoroughly rinsed with distilled water and stored in distilled water at 4 °C before characterization tests.

2.5 Characterization of NF Membranes

Membrane surface properties were explained by roughness (Zeiss optic profilometer, USA), contact angle (KSV Attension Theta, USA), zeta potential, SEM, and Fourier-transform infrared spectroscopy (FT-IR). The roughness of membrane surfaces was measured by 3D Optical Surface Profilers (Zygo New view 7100, Middlefield, CT) with at least three membranes. In the sessile drop technique used in the contact angle measurement, a drop of distilled water was dripped onto the dry membrane surface. After the drop was kept on the surface for 5 s, 10 measurements were recorded at 25 °C with 1-s intervals. The measurement was repeated by taking samples from 5 different parts of the membrane. Results are reported with the mean and standard deviation of all measurements. Zeta potential analyses (SurPASS, Anton Paar GmbH) were done by circulating 500 mL of 1.0 mM KCl feed solution at pH 8 through an adjustable gap cell containing membrane samples. Helmholtz-Smoulchowski equation was used for zeta potential calculations (Paar, 2017). A piece of membrane coupon (1×1 cm^2) was used for SEM analysis on the surface and cross-section layer. The samples were naturally air-dried and the dried samples were coated in 4.5 nm gold prior to SEM analysis. FT-IR spectroscopy (Spectrum 100, PerkinElmer, USA) was used to chemically analyze the membrane structure.

2.6 Experimental Set-up

Figure 4 shows the configurations for the treatment of wastewater.

Membrane performance tests for water permeability and real wastewater removal were determined using the Sterlitech (HP4750 models) dead-end filtration system. Before filtration experiments, membranes were compacted for 30 min at 12 bars for NF membranes to obtain stable membrane performance. After compaction, pure water was filtered through the membrane under 9 bar for NF membranes. Pure water flux was calculated according to Eq. 1. COD was measured based on SM 5220-C and the conductivity levels of the samples were determined by conductivity meter (Hach Lange). TOC was measured by Shimadzu TOC V-CPH. Removal rates of COD, conductivity, and TOC were calculated by Eq.2. A UV–vis spectrophotometer (DR5000, Hach Lange,
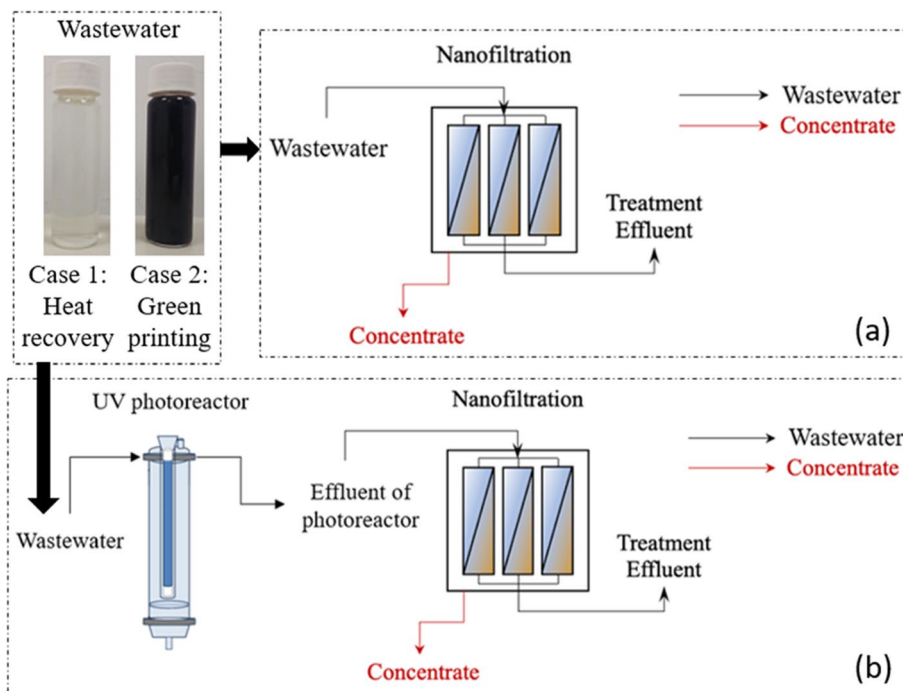
Fig. 4 NF alone membrane treatment (**a**), configuration of PC/NF treatment (**b**) for two real textile wastewater

USA) was used to absorbance at wavelengths of 436 nm, 525 nm, and 620 nm (denoted as A_{436}, A_{525}, A_{620}), and Pt–Co respectively. Chroma is denoted as color number (CN) and calculated in Eq. 3.

$$PWF(Lm^{-2}h^{-1}) = \frac{m_{water}}{t_{elapsed} * \rho_{water} * A_{membrane}} \quad (1)$$

$$R(\%) = \left(1 - \frac{C_{permeate}}{C_{feed}}\right)x100 \quad (2)$$

$$CN = \frac{A_{436}^2 + A_{525}^2 + A_{620}^2}{A_{436} + A_{525} + A_{620}} \quad (3)$$

3 Results and Discussion

Two wastewater matrices with different compositions were initially tested and compared in terms of dye and organic matter degradation and conductivity rejection by NF following PC pretreatment. In the PC step, TiO$_2$/HNT nanoparticle was synthesized,

characterized, and used as a photocatalyst in a fluidized bed photoreactor. In the NF process, novel membranes including variable monomers and nanoparticles were fabricated and described morphological properties.

### 3.1 Characterization and Photocatalytic Activity Test of TiO$_2$/HNT

The structure and morphology of raw HNT and TiO$_2$/HNT nanoparticles were characterized by FE-SEM. As shown in Fig. 5b, the surface of HNT has been successfully coated with TiO$_2$ nanoparticles using the hydrothermal method. After coating with TiO$_2$ nanoparticles, it is obvious that the dispersion is homogeneous and the cylindrical structure of HNT nanotubes is preserved.

The morphological structures of TiO$_2$/HNT nanocomposites were characterized by HRTEM. The HRTEM images of the nanocomposite structures are shown in Fig. 6. The size of the hollow HNT nanotubes was found to be about 1.2 μm, and the inner and outer diameters of the tubes were found to about 10 and 50 nm, respectively. The TiO$_2$
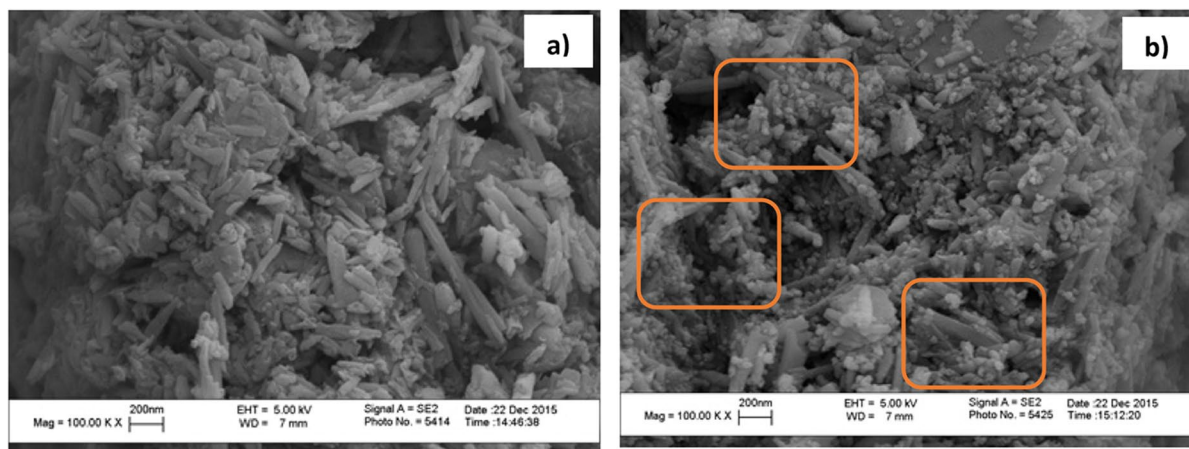
Fig. 5 SEM images of HNT (**a**), and TiO$_2$/HNT (**b**)

**Fig. 6** HRTEM and mapping images of TiO$_2$/HNT
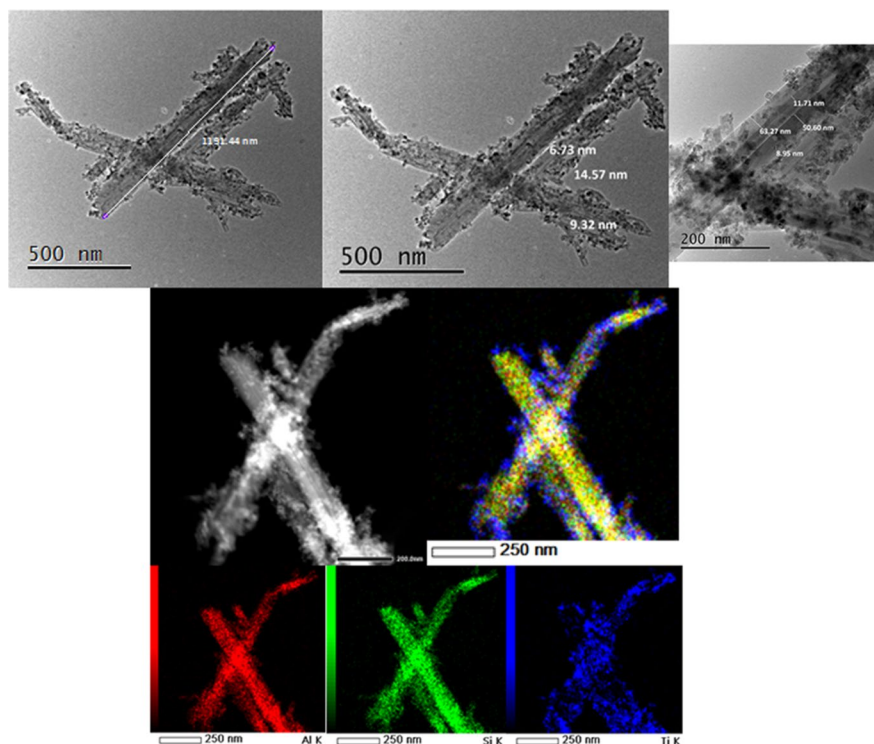
nanoparticles attached to the surface of the HNT nanotubes by hydrogen bonding were found to be dispersed throughout the HNT tubes, and the nanoparticle size was found to vary between 6 and 15 nm.

The adsorption and photocatalytic degradation figures of RO16 (100 ppm) and SR120 (200 ppm) chemical dyes on raw HNT and TiO$_2$/HNT (2 g/L) are shown in Fig. 7. Considering the photocatalytic

degradation values, when the photocatalyst was HNTs, 73.98% of the 173 ppm SR120 concentration remaining after adsorption was degraded in 12 h and 83.81% in 16 h as a result of UV interaction. On the other hand, when TiO$_2$/HNTs were used as a photocatalyst, 97.9% of the 175.9 ppm concentration of SR120 remaining after adsorption was degraded in 12 h and almost 100% in 16 h as a result of interaction

Fig. 7 Adsorption and photocatalytic degradation of HNTs and TiO$_2$/HNT for setazol red 120 (SR120) and reactive orange 16 (RO16)
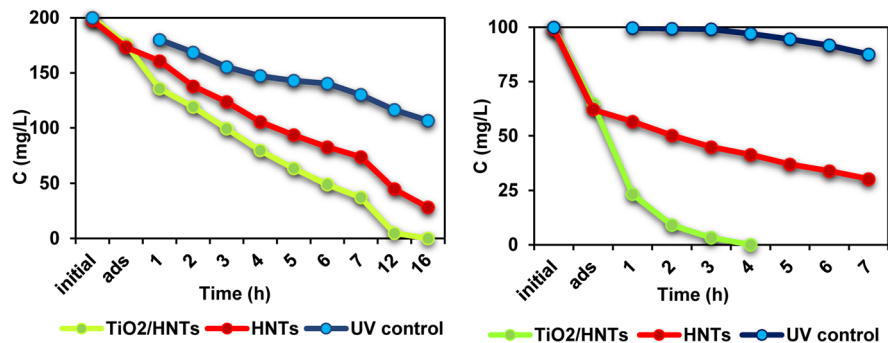
with UV. In the UV control experiment, 46.5% of the SR120 was degraded. As a result, TiO$_2$/HNT material provided 100% removal of SR120 when photocatalyzed by UV. While the adsorption of HNT photocatalyst was 37.37% in 24 h, this value was found to be 35% when TiO$_2$/HNTs were used. In terms of photocatalytic degradation, only HNT degraded 51.52% of the 62.1 ppm RO16 concentration remaining after adsorption at the end of 7 h as a result of UV photodegradation. Besides, almost 100% of the 62.5 ppm concentration of RO16 remaining after TiO$_2$/HNT adsorption was degraded as a result of UV treatment for 7 h. In the UV control set, 12.41% of the RO16 was degraded after 7 h photodegradation. Consequently, TiO$_2$/HNT material provided 100% removal of RO16 when photocatalyzed by UV. According to Du et al., after 4 h of UV irradiation, a TiO$_2$/HNT composite made using the sol–gel technique degraded 81.6% of methylene blue (Du & Zheng, 2014).

The photochemical processes occur when TiO$_2$ nanoparticles are irradiated with UV light in the presence of HNTs (Mishra & Mukhopadhyay, 2019). HNTs act as electrical insulators, preventing charge transfer during UV irradiation and contributing to the efficient movement and separation of electrons (e$^-$) and holes (h$^{+)}$) on the TiO$_2$ surface. Additionally, HNTs enhance dye degradation by bringing dye molecules closer to TiO$_2$ through electrostatic forces. Upon UV irradiation, a photoelectron is generated, creating a hole in the valence band and an electron in the conduction band of TiO$_2$/HNTs. These photogenerated electrons reduce Ti^{+4}/HNTs cations, while holes oxidize O^{2-}* anions, leading to the production of OH* radicals. These radicals act as potent oxidizing agents, degrading organic molecules adsorbed on the TiO$_2$/HNT surface and present in the surrounding environment. Simultaneously, O$_2$ voids are created

on the surface, filled by water molecules, resulting in increased surface hydrophilicity. The efficiency of organic molecule breakdown depends on their stability and structure. The electrons in the conduction band react with O$_2$, generating superoxide radicals (O$_2-$*), which accelerate the oxidation process and prevent electron/hole recombination. The formation of highly reactive hydroxyl radicals (OH*) through the reaction of H + with O$_2-$* contributes to pollutant degradation (Abid & A. Ben Haj Amara, M. Bechelany, 2023).

3.2 Characterization of Membranes

The characterization results of the fabricated membranes are given in Table 2. The membranes utilized were also a part of our group's earlier research; nevertheless, to aid in comprehension, the membrane characterization outcomes were also provided within the parameters of this research, with pertinent group articles cited for each outcome.

Optic profilometry was used to determine the roughness of all membrane surfaces. Analysis was repeated with at least three different membrane samples. It is expected that the membrane surface roughness will increase with the expansion of the surface area. Rougher surfaces provide an increase in the hydrophilicity, and an enhancement of the water flux of the membrane (Freger, 2003; Hirose et al., 1996). As presented in Table 2, according to the roughness results, it was understood that %0.04 cycloHNT TFN has the roughest surface. Hydrophilicity is also an important parameter that gives an idea about flux.

In order to determine the membrane hydrophilicity, contact angle measurements were made for all membranes produced. The average results of contact angle measurements are given in Table 2. The contact

Table 2 Characterization results of membranes

| Membrane	Contact angle (°)	Zeta potential (mV)	Roughness (RMS)	Reference
Bare PIP TFC	41.60 ± 2.20	-59.34	0.24	Ormanci-Acar et al., 2020)
%80 s-DADPS TFC	32.10 ± 0.35	-75.26	0.13	Ormanci-Acar et al., 2020)
%0.02 HNT TFN	40.90 ± 2.50	-71.40	0.20	Ormanci-Acar et al., 2021)
%0.04 cycloHNT TFN	48.00 ± 2.60	-59.73	0.30	Ormanci-Acar et al., 2018)
%80 s-DADPS %0.01HNT TFN	34.50 ± 0.20	-85.34	0.24	Ormancı-Acar et al., 2022)

angle of flat and smooth surfaces is higher than the ridge-and-valley surfaces (Wang et al., 2014). Supporting this knowledge, the %0.04 cycloHNT TFN had the highest contact angle.

Besides, the molecular weight of s-DADPS (673 g/mol) is considerably higher than that of PIP (86.14 g/mol). It is thought that this causes the transport of amine monomers to the organic phase (the phase containing TMC monomer) to be slower (Akbari et al., 2016; Song et al., 2005). Thus, since the IP takes place more slowly, a thinner and flawless layer can be obtained. If the improvement in the contact angle is considered in general, it can be said that this increase in hydrophilicity increases with the amount of carboxylic groups released as a result of the partial hydrolysis of the acyl chloride agent of the TMC monomer (Wei et al., 2013). Membranes containing s-DADPS monomer have lower both roughness and contact angle values. However, as can be seen in Table 2, HNT-added membranes became rougher and more hydrophilic (Ormanci-Acar et al., 2018).

As the negative charge of the produced membrane surface increases, the dye removal efficiency also increases. It is anticipated that membrane fouling from textile wastewaters containing negatively charged ions might be effectively prevented due to the higher negative surface charge of TFN membranes. The surface charge of the membranes was determined by zeta potential analysis. Zeta potential analysis is an important analysis that effectively and reliably determines the surface charge of membranes. Due to the unique structure of the NF membrane, the separation capacity varies depending on the steric effect due to small pore diameters and the charge on the pore surface (Donnan, 1924; Seidel et al., 2001). Positron annihilation lifetime spectroscopy measurements reveal that the porosity of commercial NF membranes varies from 1.3% (membrane active layer polyamide)

to 9.7% (membrane active layer polyethersulfone) (Boussu et al., 2007). The surface porosity can also be found by calculating the ratio of the area of the pores to the total area, which is 11.7% for NF270 and 17.1% for NF90 (Hilal et al., 2005). Since it is known that NF membranes generally have a negative charge (Schaep et al., 1998), Table 2 shows that the produced membranes also have negative surface charges at pH=8–8,4. Carboxylic and sulfonic acid groups from TMC and s-DADPS are effective in making the surface more negative. These functional groups are hydrolyzed to their protons at natural pH and become more negative as the pH rises. Many studies say that pH change has an effect on the membrane load, depending on the separation of functional groups (Bellona et al., 2004; Childress & Elimelech, 1996; Schaep et al., 1998; Tiraferri & Elimelech, 2012). Hu et al. (2016) stated that the -SO$_3$H groups in the sulfonated monomer increase the negative groups of the membrane surface (Hu et al., 2016). The -SO$_3$H groups in the s-DADPS monomer employed in this research exhibit the same effect.

FT-IR was used to determine the functional groups of NF membranes. The results obtained are given in Fig. 8. The IR bands at 1322 cm^{-1}, 1292 cm^{-1}, 1238 cm^{-1}, and 1148 cm^{-1} show typical polysulfone polymer characteristics (Misdan et al., 2013). The peak at 1639 cm^{-1} shows the interfacial polymerization, i.e., the C=O band. In addition, the jump of the C-N amide group located in the peak at 1584 cm^{-1} provides evidence for successful interfacial polymerization (Veerababu et al., 2014). Symmetric and asymmetric stretching of S=O bonds emerges in the peak at 1311 cm^{-1} (Akbari et al., 2016). The peaks at 1013 cm^{-1} and 1079 cm^{-1} show the jumping of the sulfonate groups of the s-DADPS monomer (Akbari et al., 2016). 1003.74, 908.11, and 748.17 cm^{-1} bands indicate the presence of HNT (Theng et al., 1982).

Fig. 8 FT-IR spectrum of fabricated NF membranes
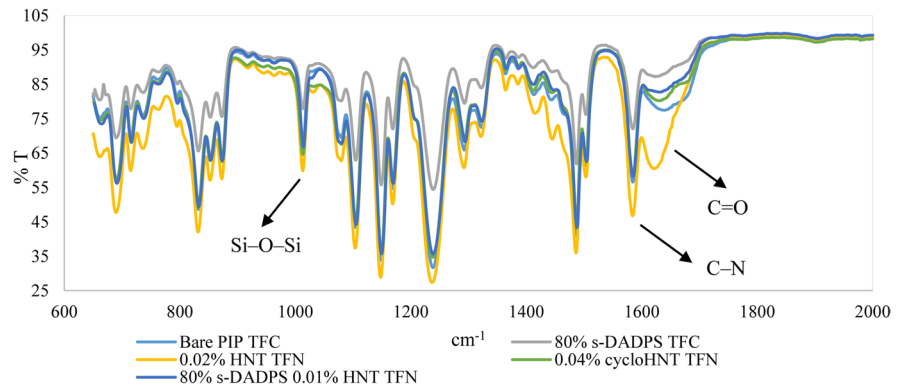
The 1003.74 cm^{-1} peak shows the Si–O-Si vibrations of HNT (Bordeepong et al., 2011). The vibration at 912 cm^{-1} represents the hydroxyl groups responsible for the presence of HNT. The peak at 748 cm^{-1} is indicative of the Al–OH surface hydroxyl groups of HNT (Farmer, 1974; Frost, 1995).

The surface morphologies of whole NF membranes were examined by SEM and the images obtained are given in Fig. 9. When the surface images are examined, it is noteworthy that the surface of the bare PIP (0%) membrane is less smooth. As the HNT ratio increases, wavy structures form on the surface, making the membrane surface rougher when Fig. 9c and d are compared. This can be verified with RMS values 0.20 and 0.30 of 0.02% HNT and 0.04% cycloHNT respectively. It was determined that

ring-like structures were formed in the membrane containing 80% S-DADPS (Fig. 9b). With the addition of 0.01% HNT, these rings became denser, and a rougher surface was obtained, in line with Ghanbari and Mozia et al. work (Ghanbari et al., 2015; Mozia et al., 2019) (Fig. 9e).

3.3 Performance Results of PC/NF and Alone NF Processes

3.3.1 Heat Recovery Wastewater

In this case, two processes were applied for the treatment of the WW from the heat recovery process. Firstly, raw wastewater was fed to a UV photocatalytic reactor (PC) as a pretreatment step. Then, the

Fig. 9 SEM images of NF membranes (**A** bare PIP TFC, **B** %80 s-DADPS TFC, **C** %0.02 HNT TFN, **D** %0.04 cycloHNT TFN, **E** %80 s-DADPS %0.01HNT TFN)
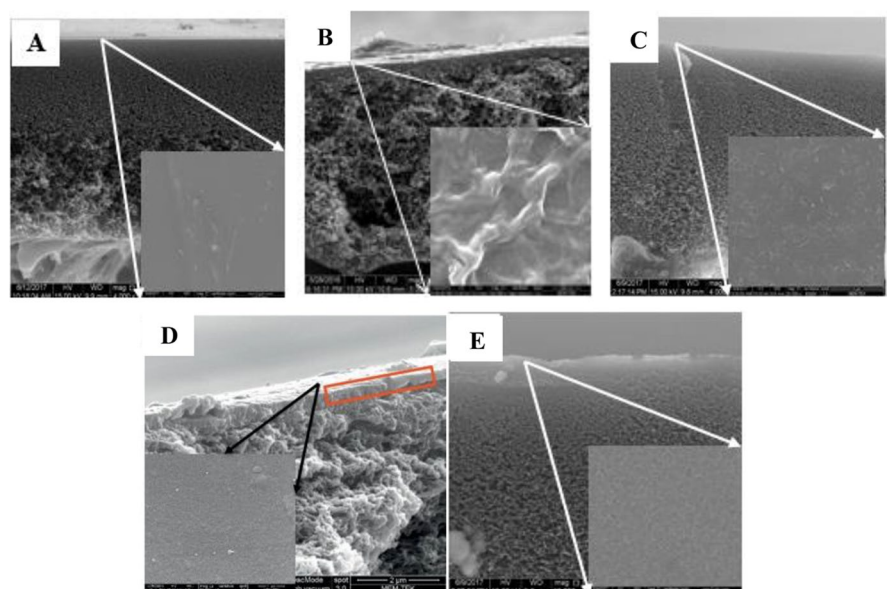
effluent from the PC was used as a feed solution for TFC and TFN NF membranes produced in this research. In the second process, raw wastewater was fed to alone NF membranes directly. The WW fluxes and the removal efficiencies of COD, conductivity, and color were compared to determine the effects of pretreatment. The treatment performance and effluent characteristics of the PC process are shown in Table 3. COD removal was achieved > 90% in wastewater completely decolorized with PC. However, a significant amount of COD concentration remained in the effluent. HNT can be utilized as support to reduce TiO_2 agglomeration and raise the specific surface area (and subsequently the absorbance and catalytic activity), as several groups have shown (Wang et al., 2011). In Alinsafi et al.'s (2007) study, the COD removal reached a maximum of 90% by UV photocatalysis in textile WW (Alinsafi et al., 2007). After PC, the pH value of WW decreased to 3.58. The representation of the dye degradation mechanism by hydroxyl radicals (OH•) is articulated as follows (Fig. 10).

Furthermore, when the pH value was above 10, the average reaction rate increased. This is because when the solution is sufficiently alkaline (pH values more than 10), the increased concentration of OH dot radicals increases the degradation rate. The findings align with Wei and Wan's research on the photocatalytic oxidation of phenol, emphasizing that a pH above 10 facilitates a more rapid degradation of organic compounds (Wei & Wan, 1991). The efficacy of chemical oxygen demand (COD) exhibited a discernible decline as the initial concentration increased. This phenomenon can be attributed to the heightened concentration of dye and COD, resulting in an intensified coloration of the solution. Consequently, the diminished path length of photons entering the solution contributes to a reduced number of photons reaching the catalyst surface (Castillo-Suárez et al., 2023; Uma et al., 2019).
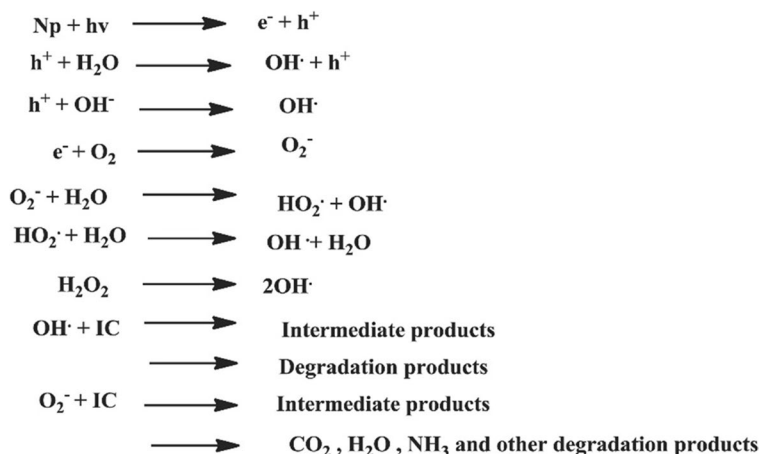
The NF flux performance analysis made with PC effluent is given in Fig. 11. The s-DADPS monomer causes macrovoid formation during cross-linking because its molecular weight is higher than that of PIP. In addition, since the s-DADPS monomer contains sodium sulfonate ($NaSO_3$) ionic groups, the electrostatic surface of the membranes is negatively charged. The electrostatic surface changing and macrovoid spaces forming provide a more hydrophilic membrane and enhance salt and dye removal efficiency.

The color removal efficiencies were 100% for all types of membranes. There was no difference

Table 3 Characterization of PC effluent and the removal efficiency of PC

Parameter	Heat recovery wastewater	
	PC effluent	Removal efficiency, %
COD, mg/L	326	90.6
Conductivity, μs/cm	2270	33.2
CN	0	100

Fig. 10 Mechanism of dye degradation by OH radical (Uma et al., 2019)

$$Np + hv \longrightarrow e^- + h^+$$
$$h^+ + H_2O \longrightarrow OH\cdot + h^+$$
$$h^+ + OH^- \longrightarrow OH\cdot$$
$$e^- + O_2 \longrightarrow O_2^-$$
$$O_2^- + H_2O \longrightarrow HO_2\cdot + OH\cdot$$
$$HO_2\cdot + H_2O \longrightarrow OH\cdot + H_2O$$
$$H_2O_2 \longrightarrow 2OH\cdot$$
$$OH\cdot + IC \longrightarrow \text{Intermediate products}$$
$$\longrightarrow \text{Degradation products}$$
$$O_2^- + IC \longrightarrow \text{Intermediate products}$$
$$\longrightarrow CO_2, H_2O, NH_3 \text{ and other degradation products}$$

Fig. 11 The flux of WW from heat recovery process produced by NF permeate with and without PC pretreatment
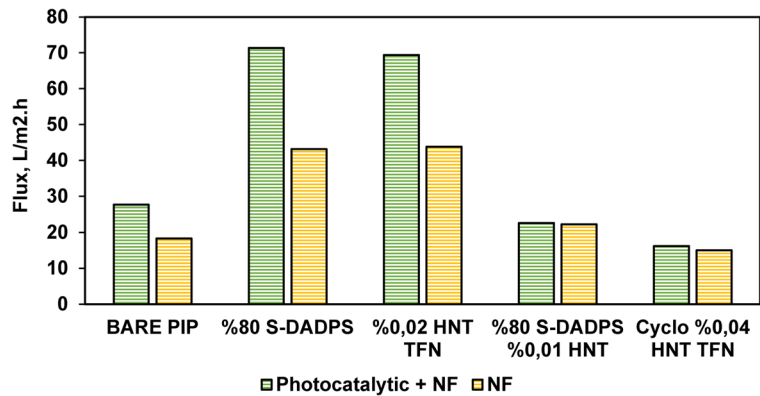
between the two processes. COD and conductivity levels were used to characterize the content of organic and ionic substances in WW, respectively, and to reflect the degree of water pollution. Table 4 shows that the rejections to COD in the heat recovery WW were enhanced by the PC pretreatment. There was no difference in COD removal with these NF membranes in terms of concentration in the effluent and removal efficiency. This proved the positive contribution of PC pretreatment in terms of effluent concentrations.

The results show that PC pretreatment led to a tenfold decrease in COD values in the effluent (Table 4). Also, conductivity values were lower in the pretreated effluent compared to the non-pretreated effluent (Table 5). Notably, the bare PIP TFC membrane achieved a 95–96% success rate in conductivity removal. Furthermore, PC pretreatment of the bare PIP TFC membrane increased the flux from 18.3 to 27.6 L/m^2.h (Fig. 11).

3.3.2 Printing Wastewater

The other WW was obtained from the green printing process in the cotton textile industry (Table 6). The COD removal efficiency was succeeded at > 96% rate in a similar heat recovery WW case. After PC pretreatment, pH was declined heavily to 2.60.

The flux values of NF membranes are portrayed in Fig. 12. Sulfonation is one of the most frequently used and one of the most important chemical modification processes used for polymeric materials. The sulfonation process can be defined as the covalent bonding of the sulfonic (-SO$_3$H) group to the polymer chain. The sulfone group that enters the polymer structure gives the material very unusual and beneficial properties compared to its pre-modification properties such as good wettability, water solubility, ion exchange and transfer properties, and membrane properties. Considering this, the high flux obtained in TFC and TFN membranes containing 80% S-DADPS shows that the additive

Table 4 COD levels of permeate and removal rates for heat recovery WW

	COD			
	Effluent, mg/L	Removal efficiency, %	Effluent, mg/L	Removal efficiency, %
	NF alone		PC + NF	
Bare PIP TFC	75.6	97.8	7.0	99.8
80% s-DADPS TFC	72.9	97.9	6.9	99.8
0.02% HNT TFN	74.6	97.9	7.1	99.8
0.04% cycloHNT TFN	76.3	97.8	7.1	99.8
80% s-DADPS 0.01% HNT TFN	76.0	97.8	7.1	99.8

Table 5 Conductivity levels of permeate and removal rates for heat recovery WW

	Conductivity			
	Effluent, μs/cm	Removal efficiency, %	Effluent, μs/cm	Removal efficiency, %
	NF alone		PC + NF	
Bare PIP TFC	132	96.1	168	95.1
%80 s-DADPS TFC	2440	28.5	1895	44.3
%0.02 HNT TFN	2230	34.4	1760	48.2
%0.04 cycloHNT TFN	1312	61.4	1482	56.4
%80 s-DADPS %0.01HNT TFN	785	76.9	1405	58.7

Table 6 Performance results after photocatalytic reactor pretreatment

Parameter	Green printing	
	Effluent	Removal efficiency, %
COD, mg/L O$_2$	37.2	96.3
Conductivity, μs/cm	6937	22.0
CN	0	100

is in place. It also gave similar results with the flux values in the literature (Xie et al., 2012). It is thought that the sulphonic groups contained in the S-DADPS monomer increase the water passage through the membrane. On the other hand, it is thought that a thinner layer is formed because the S-DADPS monomer, which has a higher molecular weight, passes into the organic phase more slowly (Xie et al., 2012).

It was observed that PC pretreatment slightly reduces the flux (Fig. 12). However, the surface of HNT is negatively charged when the pH is above 2.4. Thus, positively charged particles can be easily absorbed onto HNT and decomposed effectively (Isari et al., 2018). According to the results of TFN NF membrane tests, the introduction of HNT in the active layer reduced flux values but did not affect removal efficiencies significantly as it is compatible with the literature (Tables 7 and 8) (Mozia et al., 2019).

When Table 7 is examined, it was understood that NF membranes were quite successful in organic matter removal. Again, 80% S-DADPS TFC membrane had the highest values among other membranes with 98% and 86%. It was followed by high-efficiency HNT-doped membranes. It was seen that both flux and efficiency improvement were achieved. The "steric effect" and the "charge effect" are both involved in the NF membrane separation mechanism. It is achievable to reject charged

Fig. 12 The flux of wastewater from green printing process produced by NF permeate with and without photocatalytic pretreatment
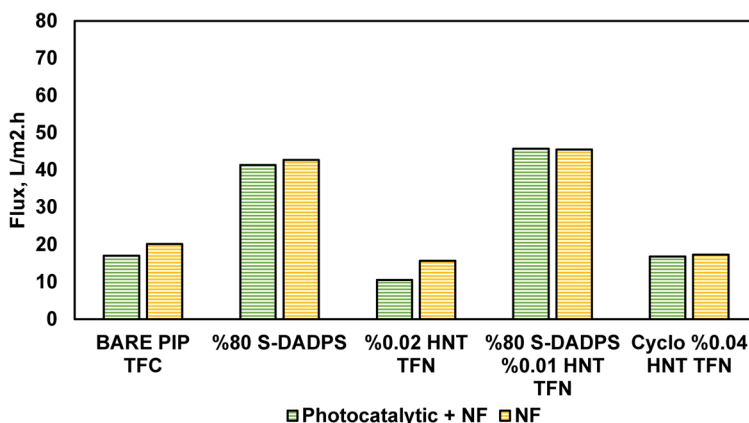
Table 7 COD levels of permeate and removal efficiencies for printing WW

	COD			
	Effluent, mg/L	Removal efficiency, %	Effluent, mg/L	Removal efficiency, %
	NF alone		PC + NF	
Bare PIP TFC	79.2	92.1	21.2	97.9
80% s-DADPS TFC	11.6	98.8	18.6	98.1
0.02% HNT TFN	86.0	91.4	20.9	97.9
0.04% cycloHNT TFN	3.9	99.6	14.8	98.5
80% s-DADPS 0.01% HNT TFN	48.3	95.2	20.2	98.0

Table 8 Conductivity levels of permeate and removal efficiencies for printing WW

	Conductivity			
	Effluent, µs/cm	Removal efficiency, %	Effluent, µs/cm	Removal efficiency, %
	NF alone		PC + NF	
Bare PIP TFC	890	90.0	3570	59.7
%80 s-DADPS TFC	2390	73.1	2726	69.2
%0.02 HNT TFN	2300	74.1	5200	41.4
%0.04 cycloHNT TFN	4010	54.8	4305	51.5
%80 s-DADPS %0.01HNT TFN	4295	51.5	4650	47.6

solutes that are larger than the membrane pores. Multivalent negative ions are generally separated by NF membranes with a greater rejection degree than monovalent ions. This could make it conceivable to extract ions from wastewater and divide them according to their ionic valences (Fievet et al., 2002). It can be said that the moderate performance of doped membranes in conductivity removal is due to the fact that textile wastewater contains monovalent salts rather than divalent salts (Table 8).

Color removal in wastewater during the photocatalysis process is the result of decreased concentration of the dyes as well as the cleavage of the -N=N- bond, which determines the colors of the dyes. Removal of color does not mean that organic matter has been completely removed from the treated solutions. The decomposition of dyes can lead to smaller organic molecules that do not provide coloring, but organic matter is still present in the solution (Ormancı-Acar et al., 2022). Since the dye substances are purified in the photocatalytic reactor, there is no decolorization load left for the NF process.

Considering the overall results of the study, the optimum PC + NF combination in terms of treatment and filtration performances is compared in Table 9. In heat recovery WW treatment, although the highest flux was obtained with %80 s-DADPS TFC NF recorded as approximately 71.4 L/m^2.h, the best treatment performance was obtained by bare PIP TFC NF membrane. In NF treatment in printing WW, the 80% s-DADPS TFC NF membrane provided a flux of 42.7 L/m^2.h. The removal efficiency of organic matter was 98.1%, while the conductivity was 73.1%. Compared to other studies using TiO$_2$, almost two times higher results were obtained in terms of treatment performance.

4 Conclusion

The use of TiO$_2$/HNT in real wastewater with UV photocatalysis was the first in the literature with this study. TiO$_2$/HNT, selected as a photocatalyst, showed that it has a higher degradation potential than raw

Table 9 Comparison with the literature

Photocatalyst type	UV source	Membrane type	Feed water	Performance	References
Immobilized bed P25 TiO$_2$, Degussa	Mercury lamp emitting UV-A light (λmax = 355 nm)	Desal DK5	10 mg/L Acid Red 18 (AR18), Direct Green 99 (DG99), and Acid Yellow 36 (AY36)	Conductivity, TDS, TOC removals of 65%, 50%, 10% respectively	Grzechulska-Damszel et al., 2009
TiO$_2$	Low-pressure mercury vapor lamp (maximum emission at 365 nm)	M/s TAMI Industries ceramic NF membrane	Brilliant Green (BG)	Flux: 60 L/m^2.h; 99% decolorization	Donkadokula et al., 2020
TiO$_2$	UV lamp 40 W	NF270	Textile industry washing process	Conductivity, COD, color removals of 75% 5%, 100%	Özgün et al., 2023
TiO$_2$/HNT	UV-C light (λmax = 253.7 nm)	Bare PIP TFC	Textile industry heat recovery process	Flux: 27.6 L/m^2.h; complete decolorization; 99.8% of COD, 95.1% of conductivity removal	This work
TiO$_2$/HNT	UV-C light (λmax = 253.7 nm)	%80 s-DADPS TFN NF	Textile industry printing process	Flux: 42.7 L/m^2.h; complete decolorization; 98.1% of COD, 73.1% of conductivity removal	This work

HNT in characterization tests. In tests conducted with real wastewater, it provided complete decolorization. The results obtained in this study showed that photocatalytic treatment is totally efficient in removing the dye substances in real wastewater sources that have different compositions.

In heat recovery wastewater, the combination of UV photocatalysis and nanofiltration allows the production of water of higher quality than the individual processes with global removals in COD higher than 99% for all fabricated novel membranes. Almost 100% COD removal was achieved. Conductivity removal performance remained in the 50% band with NF membranes after pretreatment. Bare PIP membrane was > 95% effective in conductivity removal. It can be said that the moderate performance of doped membranes in conductivity removal is due to the fact that textile wastewater contains monovalent salts rather than divalent salts. Steady flux increased with pretreatment in bare and noval TFN membranes at varying degrees.

As a result of PC + NF and NF studies performed on the printing wastewater sample, > 98% COD removal was achieved. It has been determined that PC pretreatment does not have a dominant contribution to conductivity removal. But, treated wastewater quality was significantly enhanced in terms of COD and color.

If color removal was the basic goal of this work, the increase in COD removal is an additional positive factor, as it would improve the efficiency of a NF process. No pH adjustment is necessary and wastewater at high pH can be treated directly after suspended solids removal.

Declarations

References

Abdullayev, E., Price, R., Shchukin, D., & Lvov, Y. (2009). Halloysite tubes as nanocontainers for anticorrosion coating with benzotriazole. *ACS Applied Materials & Interfaces, 1*, 1437–1443. https://doi.org/10.1021/am9002028

M. Abid, A. Ben Haj Amara, M. Bechelany, Halloysite-TiO2 nanocomposites for water treatment: A review, *Nanomaterials*. 13 (2023). https://doi.org/10.3390/nano13091578.

S. Aftab, T. Shabir, A. Shah, J. Nisar, I. Shah, H. Muhammad, N.S. Shah, Highly efficient visible light active doped ZnO photocatalysts for the treatment of wastewater contaminated with dyes and pathogens of emerging concern, *Nanomaterials*. 12 (2022). https://doi.org/10.3390/nano12030486.

Agtaş, M., Ormancı-Acar, T., Keskin, B., Türken, T., & Koyuncu, I. (2021). Nanofiltration membranes for salt and dye filtration: Effect of membrane properties on performances. *Water Science and Technology, 83*, 2146–2159. https://doi.org/10.2166/wst.2021.125

Ağtaş, M., Yılmaz, Ö., Dilaver, M., Alp, K., & Koyuncu, İ. (2020). Hot water recovery and reuse in textile sector with pilot scale ceramic ultrafiltration/nanofiltration membrane system. *Journal of Cleaner Production, 256*, 1–12. https://doi.org/10.1016/j.jclepro.2020.120359

Ahmad, A., Ali, M., Al-Sehemi, A. G., Al-Ghamdi, A. A., Park, J. W., Algarni, H., & Anwer, H. (2023). Carbon-integrated semiconductor photocatalysts for removal of volatile organic compounds in indoor environments. *Chemical Engineering Journal, 452*, 139436. https://doi.org/10.1016/j.cej.2022.139436

Ahmadpour, N., Nowrouzi, M., MadadiAvargani, V., Sayadi, M. H., & Zendehboudi, S. (2024). Design and optimization of TiO2-based photocatalysts for efficient removal of pharmaceutical pollutants in water: Recent developments and challenges. *Journal of Water Process Engineering, 57*, 104597. https://doi.org/10.1016/j.jwpe.2023.104597

Akbari, A., Aliyarizadeh, E., MojallaliRostami, S. M., Homayoonfal, M., Rostami, S. M. M., & Homayoonfal, M. (2016). Novel sulfonated polyamide thin-film composite nanofiltration membranes with improved water flux and anti-fouling properties. *Desalination., 377*, 11–22. https://doi.org/10.1016/j.desal.2015.08.025

Alinsafi, A., Evenou, F., Abdulkarim, E. M., Pons, M. N., Zahraa, O., Benhammou, A., Yaacoubi, A., & Nejmeddine, A. (2007). Treatment of textile industry wastewater by supported photocatalysis. *Dyes and Pigments, 74*, 439–445. https://doi.org/10.1016/j.dyepig.2006.02.024

Baek, M. H., Yoon, J. W., Hong, J. S., & Suh, J. K. (2013). Application of TiO2-containing mesoporous spherical activated carbon in a fluidized bed photoreactor - Adsorption and photocatalytic activity. *Applied Catalysis, A: General, 450*, 222–229. https://doi.org/10.1016/j.apcata.2012.10.018

Bellona, C., Drewes, J. E., Xu, P., & Amy, G. (2004). Factors affecting the rejection of organic solutes during NF/RO treatment—a literature review. *Water Research, 38*, 2795–2809.

Bordeepong, S., Bhongsuwan, D., Pungrassami, T., Bhongsuwan, T. (2011). Characterization of halloysite from Thung Yai District, Nakhon Si Thammarat Province, in Southern Thailand. *Songklanakarin Journal of Science & Technology, 33*(5).

Boussu, K., De Baerdemaeker, J., Dauwe, C., Weber, M., Lynn, K. G., Depla, D., Aldea, S., Vankelecom, I. F. J., Vandecasteele, C., & Van Der Bruggen, B. (2007). Physicochemical characterization of nanofiltration membranes. *ChemPhysChem, 8*, 370–379. https://doi.org/10.1002/cphc.200600512

Braham, R. J., & Harris, A. T. (2009). Review of major design and scale-up considerations for solar photocatalytic reactors. *Industrial and Engineering Chemistry Research, 48*, 8890–8905.

Castillo-Suárez, L. A., Sierra-Sánchez, A. G., Linares-Hernández, I., Martínez-Miranda, V., Teutli-Sequeira, E. A. (2023). A critical review of textile industry wastewater: Green technologies for the removal of indigo dyes. *International Journal of Environmental Science and Technology,* 1–38. https://doi.org/10.1007/s13762-023-04810-2

Childress, A. E., & Elimelech, M. (1996). Effect of solution chemistry on the surface charge of polymeric reverse osmosis and nanofiltration membranes. *Journal of Membrane Science, 119*, 253–268.

Das, L., & Basu, J. K. (2015). Photocatalytic treatment of textile effluent using titania-zirconia nano composite catalyst. *Journal of Industrial and Engineering Chemistry, 24*, 245–250. https://doi.org/10.1016/j.jiec.2014.09.037

Donkadokula, N. Y., Kola, A. K., Saroj, D. (2020). Modelling and optimization studies on decolorization of brilliant green dye using integrated nanofiltration and photocatalysis. *Sustainable Environment Research,* 30. https://doi.org/10.1186/s42834-020-00050-y

Donnan, F. G. (1924). The theory of membrane equilibria. *Chemical Reviews, 1*, 73–90.

Du, Y., & Zheng, P. (2014). Adsorption and photodegradation of methylene blue on TiO2-halloysite adsorbents. *Korean Journal of Chemical Engineering, 31*, 2051–2056. https://doi.org/10.1007/s11814-014-0162-8

Evgenidou, E., Fytianos, K., & Poulios, I. (2005). Photocatalytic oxidation of dimethoate in aqueous solutions. *Journal of Photochemistry and Photobiology, A: Chemistry, 175*, 29–38.

Farmer, V. C. (1974). The layer silicates. In *The Infrared Spectra of Minerals*. https://doi.org/10.1180/mono-4.15

Fievet, P., Labbez, C., Szymczyk, A., Vidonne, A., Foissy, A., & Pagetti, J. (2002). Electrolyte transport through amphoteric nanofiltration membranes. *Chemical Engineering Science, 57*, 2921–2931. https://doi.org/10.1016/S0009-2509(02)00188-4

Freger, V. (2003). Nanoscale heterogeneity of polyamide membranes formed by interfacial polymerization. *Langmuir, 19*, 4791–4797.

Frost, R. L. (1995). Fourier transform Raman spectroscopy of kaolinite, dickite and halloysite. *Clays and Clay Minerals, 43*, 191–195.

Ghanbari, M., Emadzadeh, D., Lau, W. J., Lai, S. O., Matsuura, T., & Ismail, A. F. (2015). Synthesis and characterization of novel thin film nanocomposite (TFN) membranes embedded with halloysite nanotubes (HNTs) for water desalination. *Desalination, 358*, 33–41. https://doi.org/10.1016/j.desal.2014.11.035

Grzechulska-Damszel, J., Tomaszewska, M., Morawski, A. W. (2009). Integration of photocatalysis with membrane processes for purification of water contaminated with organic dyes. *Desalination, 241*(1-3), 118–126. https://doi.org/10.1016/j.desal.2007.11.084

Haarstrick, A., Kut, O. M., & Heinzle, E. (1996). TiO2-assisted degradation of environmentally relevant organic compounds in wastewater using a novel fluidized bed photoreactor. *Environmental Science and Technology, 30*, 817–824.

Hilal, N., Al-Zoubi, H., Darwish, N. A., & Mohammad, A. W. (2005). Characterisation of nanofiltration membranes using atomic force microscopy. *Desalination, 177*, 187–199. https://doi.org/10.1016/j.desal.2004.12.008

Hirose, M., Ito, H., & Kamiyama, Y. (1996). Effect of skin layer surface structures on the flux behaviour of RO membranes. *Journal of Membrane Science, 121*, 209–215.

Hu, J., Lv, Z., Xu, Y., Zhang, X., & Wang, L. (2016). Fabrication of a high-flux sulfonated polyamide nanofiltration membrane: Experimental and dissipative particle dynamics studies. *Journal of Membrane Science, 505*, 119–129.

Hu, J.-S., Ren, L.-L., Guo, Y.-G., Liang, H.-P., Cao, A.-M., Wan, L.-J., & Bai, C.-L. (2005). Mass production and high photocatalytic activity of ZnS nanoporous nanoparticles. *Angewandte chemie, 117*, 1295–1299.

Iqbal, J., Shah, N. S., Khan, Z. U. H., Rizwan, M., Murtaza, B., Jamil, F., Shah, A., Ullah, A., Nazzal, Y., & Howari, F. (2022). Visible light driven doped CeO2 for the treatment of pharmaceuticals in wastewater: A review. *Journal of Water Process Engineering, 49*, 103130. https://doi.org/10.1016/j.jwpe.2022.103130

Isari, A. A., Payan, A., Fattahi, M., Jorfi, S., & Kakavandi, B. (2018). Photocatalytic degradation of rhodamine B and real textile wastewater using Fe-doped TiO2 anchored on reduced graphene oxide (Fe-TiO2/rGO): Characterization and feasibility, mechanism and pathway studies. *Applied Surface Science, 462*, 549–564.

Jiang, L., Huang, Y., & Liu, T. (2015). Enhanced visible-light photocatalytic performance of electrospun carbon-doped TiO2/halloysite nanotube hybrid nanofibers. *Journal of Colloid and Interface Science, 439*, 62–68.

Kanki, T., Hamasaki, S., Sano, N., Toyoda, A., & Hirano, K. (2005). Water purification in a fluidized bed photocatalytic reactor using TiO2-coated ceramic particles. *Chemical Engineering Journal, 108*, 155–160. https://doi.org/10.1016/J.CEJ.2005.01.014

Keskin, B., Ağtaş, M., Ormancı-Acar, T., Türken, T., Imer, D. Y., Ünal, S., Menceloğlu, Y. Z., Uçar-Demir, T., & Koyuncu, I. (2021b). Halloysite nanotube blended nanocomposite ultrafiltration membranes for reactive dye removal. *Water Science and Technology, 83*, 271–283. https://doi.org/10.2166/wst.2020.573

Keskin, B., Ersahin, M. E., Ozgun, H., & Koyuncu, I. (2021a). Pilot and full-scale applications of membrane processes for textile wastewater treatment: A critical review. *Journal of Water Process Engineering, 42*, 102172. https://doi.org/10.1016/j.jwpe.2021.102172

Korkut, S., Vatanpour, V., Koyuncu, I. (2023). Carbon-based quantum dots in fabrication and modification of membranes: A review. *Separation and Purification Technology*, 124876. https://doi.org/10.1016/j.seppur.2023.124876

Li, M., Wang, X., Porter, C. J., Cheng, W., Zhang, X., Wang, L., & Elimelech, M. (2019). Concentration and recovery of dyes from textile wastewater using a self-standing, support-free forward osmosis membrane. *Environmental Science and Technology, 53*, 3078–3086.

Mahmoodi, N. M., & Arami, M. (2009). Degradation and toxicity reduction of textile wastewater using immobilized titania nanophotocatalysis. *Journal of Photochemistry and Photobiology, B: Biology, 94*, 20–24.

Misdan, N., Lau, W. J., Ismail, A. F., & Matsuura, T. (2013). Formation of thin film composite nanofiltration membrane: Effect of polysulfone substrate characteristics. *Desalination, 329*, 9–18.

Mishra, G., & Mukhopadhyay, M. (2019). TiO2 decorated functionalized halloysite nanotubes (TiO2@ HNTs) and photocatalytic PVC membranes synthesis, characterization and its application in water treatment. *Science and Reports, 9*, 4345. https://doi.org/10.1038/s41598-019-40775-4

Mozia, S., Grylewicz, A., Zgrzebnicki, M., Darowna, D., & Czyżewski, A. (2019). Investigations on the properties and performance of mixed-matrix polyethersulfone membranes modified with halloysite nanotubes. *Polymers (Basel), 11*, 671.

Naseem, T., & Durrani, T. (2021). The role of some important metal oxide nanoparticles for wastewater and antibacterial applications: A review. *Environmental Chemistry and Ecotoxicology, 3*, 59–75.

T. Ormancı-Acar, S. Korkut, B. Keskin, M. Ağtaş, C.E. Taş, Ö. Mutlu-Salmanlı, T. Türken, Y.Z. Menceloğlu, S. Ünal, İ. Koyuncu, Combining S-DADPS monomer and halloysite nanotube for fabrication superior nanofiltration membrane, *Polymer (Guildf)*. 255 (2022). https://doi.org/10.1016/j.polymer.2022.125174.

Ormanci-Acar, T., Celebi, F., Keskin, B., Mutlu-Salmanlı, O., Agtas, M., Turken, T., Tufani, A., Imer, D. Y., Ince, G. O., & Demir, T. U. (2018). Fabrication and characterization of temperature and pH resistant thin film nanocomposite

membranes embedded with halloysite nanotubes for dye rejection. *Desalination, 429*, 20–32.

Ormanci-Acar, T., Keskin, B., Korkut, S., Mutlu-Salmanlı, O., Turken, T., Koseoglu-Imer, D. Y., Demir, T. U., Mencelo-glu, Y. Z., Unal, S., & Koyuncu, I. (2021). Fabrication of halloysite nanotubes embedded thin film nanocomposite membranes for dye removal. *Journal of Applied Polymer Science, 138*, 1–12. https://doi.org/10.1002/app.50986

Ormanci-Acar, T., Tas, C. E., Keskin, B., Ozbulut, E. B. S., Turken, T., Imer, D., Tufekci, N., Menceloglu, Y. Z., Unal, S., & Koyuncu, I. (2020). Thin-film composite nanofiltration membranes with high flux and dye rejection fabricated from disulfonated diamine monomer. *Journal of Membrane Science, 608*, 118172. https://doi.org/10.1016/j.memsci.2020.118172

Özgün, H., Sakar, H., Ağtaş, M., & Koyuncu, I. (2023). Investigation of pre-treatment techniques to improve membrane performance in real textile wastewater treatment. *International Journal of Environmental Science and Technology, 20*, 1539–1550. https://doi.org/10.1007/s13762-022-04034-w

Paar, A. (2017). Viskozimetr Pod. Stabingera.

Pozzo, R. L., Conte, L. O., Giombi, J. L., & Baltanas, M. A. (2011). Photocatalytic reduction of Cr (VI) in a fully illuminated fluidized bed reactor. *Water Science and Technology, 64*, 2370–2375.

Qamar, M. A., Javed, M., Shahid, S., Shariq, M., Fadhali, M. M., Ali, S. K., & Khan, M. S. (2023). Synthesis and applications of graphitic carbon nitride (g-C3N4) based membranes for wastewater treatment: A critical review. *Heliyon, 9*, e12685. https://doi.org/10.1016/j.heliyon.2022.e12685

Qi, K., Cheng, B., Yu, J., & Ho, W. (2017). Review on the improvement of the photocatalytic and antibacterial activities of ZnO. *Journal of Alloys and Compounds, 727*, 792–820. https://doi.org/10.1016/J.JALLCOM.2017.08.142

Schaep, J., Van Der Bruggen, B., Vandecasteele, C., & Wilms, D. (1998). Influence of ion size and charge in nanofiltration. *Separation and Purification Technology, 14*, 155–162. https://doi.org/10.1016/S1383-5866(98)00070-7

Seidel, A., Waypa, J. J., & Elimelech, M. (2001). Role of charge (Donnan) exclusion in removal of arsenic from water by a negatively charged porous nanofiltration membrane. *Environmental Engineering Science, 18*, 105–113. https://doi.org/10.1089/10928750151132311

Song, Y., Sun, P., Henry, L. L., & Sun, B. (2005). Mechanisms of structure and performance controlled thin film composite membrane formation via interfacial polymerization process. *Journal of Membrane Science, 251*, 67–79.

Theng, B. K. G., Russell, M., Churchman, G. J., & Parfitt, R. L. (1982). Surface properties of allophane, halloysite, and imogolite. *Clays and Clay Minerals, 30*, 143–149.

Tiraferri, A., & Elimelech, M. (2012). Direct quantification of negatively charged functional groups on membrane surfaces. *Journal of Membrane Science, 389*, 499–508.

Uma, H. B., Ananda, S., & Nandaprakash, M. B. (2019). High efficient photocatalytic treatment of textile dye and antibacterial activity via electrochemically synthesized Ni-doped ZnO nano photocatalysts. *Chemical Data Collections, 24*, 100301.

Veerababu, P., Vyas, B. B., Singh, P. S., & Ray, P. (2014). Limiting thickness of polyamide-polysulfone thin-film-composite nanofiltration membrane. *Desalination, 346*, 19–29. https://doi.org/10.1016/j.desal.2014.05.007

Wang, C.-F., Hung, S.-W., Kuo, S.-W., & Chang, C.-J. (2014). Combining hierarchical surface roughness with fluorinated surface chemistry to preserve superhydrophobicity after organic contamination. *Applied Surface Science, 320*, 658–663.

Wang, R., Jiang, G., Ding, Y., Wang, Y., Sun, X., Wang, X., & Chen, W. (2011). Photocatalytic activity of heterostructures based on TiO2 and halloysite nanotubes. *ACS Applied Materials & Interfaces, 3*, 4154–4158.

Wei, T. Y., & Wan, C. C. (1991). Heterogeneous photocatalytic oxidation of phenol with titanium dioxide powders. *Industrial and Engineering Chemistry Research, 30*, 1293–1300.

Wei, X., Kong, X., Sun, C., & Chen, J. (2013). Characterization and application of a thin-film composite nanofiltration hollow fiber membrane for dye desalination and concentration. *Chemical Engineering Journal, 223*, 172–182. https://doi.org/10.1016/j.cej.2013.03.021

Xie, W., Geise, G. M., Freeman, B. D., Lee, H.-S., Byun, G., & McGrath, J. E. (2012). Polyamide interfacial composite membranes prepared from m-phenylene diamine, trimesoyl chloride and a new disulfonated diamine. *Journal of Membrane Science, 403*, 152–161. https://doi.org/10.1016/j.memsci.2012.02.038

Zheng, P., Du, Y., Chang, P. R., & Ma, X. (2015). Amylose–halloysite–TiO2 composites: Preparation, characterization and photodegradation. *Applied Surface Science, 329*, 256–261.

Springer